Estimating the Cross-Shelf Export of Riverine Materials
Part 1. General Relationships From an Idealized Numerical Model

Izett, Jonathan G.; Fennel, Katja

DOI
10.1002/2017GB005667

Publication date
2018

Document Version
Final published version

Published in
Global Biogeochemical Cycles

AGU PUBLICATIONS

Global Biogeochemical Cycles

RESEARCH ARTICLE
10.1002/2017GB005667

This article is a companion to Izett and Fennel (2018), https://doi.org/10.1002/2017GB005668.

Key Points:
- Numerical experiments confirm that cross-shelf export of riverine material can be predicted by the ratio of Rossby radius and shelf width
- Latitude is the dominant controlling factor in determining the efficiency of cross-shelf export on a global scale
- Simple, latitude-dependent relationships are presented to estimate plume transport across a range of different forcing scenarios

Supporting Information:
- Supporting Information S1
- Data Set S1
- Data Set S2
- Movie S1

Correspondence to:
J. G. Izett,
j.g.izett@tudelft.nl

Citation:
Izett, J. G., & Fennel, K. (2018). Estimating the cross-shelf export of riverine materials: Part 1. General relationships from an idealized numerical model. *Global Biogeochemical Cycles*, *32*. https://doi.org/10.1002/2017GB005667

Received 11 MAR 2017
Accepted 3 DEC 2017
Accepted article online 19 DEC 2017

Estimating the Cross-Shelf Export of Riverine Materials: Part 1. General Relationships From an Idealized Numerical Model

Jonathan G. Izett[1,2] **and Katja Fennel**[1]

[1]Department of Oceanography, Dalhousie University, Halifax, Nova Scotia, Canada, [2]Department of Geoscience and Remote Sensing, Delft University of Technology, Delft, The Netherlands

Abstract Rivers deliver large amounts of terrestrially derived materials (such as nutrients, sediments, and pollutants) to the coastal ocean, but a global quantification of the fate of this delivery is lacking. Nutrients can accumulate on shelves, potentially driving high levels of primary production with negative consequences like hypoxia, or be exported across the shelf to the open ocean where impacts are minimized. Global biogeochemical models cannot resolve the relatively small-scale processes governing river plume dynamics and cross-shelf export; instead, river inputs are often parameterized assuming an "all or nothing" approach. Recently, Sharples et al. (2017), https://doi.org/10.1002/2016GB005483 proposed the S_P number—a dimensionless number relating the estimated size of a plume as a function of latitude to the local shelf width—as a simple estimator of cross-shelf export. We extend their work, which is solely based on theoretical and empirical scaling arguments, and address some of its limitations using a numerical model of an idealized river plume. In a large number of simulations, we test whether the S_P number can accurately describe export in unforced cases and with tidal and wind forcings imposed. Our numerical experiments confirm that the S_P number can be used to estimate export and enable refinement of the quantitative relationships proposed by Sharples et al. We show that, in general, external forcing has only a weak influence compared to latitude and derive empirical relationships from the results of the numerical experiments that can be used to estimate riverine freshwater export to the open ocean.

1. Introduction

Freshwater plumes resulting from river discharge are common features of the world's coastal oceans. They contain not only fresh water but also terrestrially derived materials (e.g., from erosion, weathering, agricultural runoff, and urban and industrial activities) including nutrients, sediments, and pollutants. It is unclear, however, how much of this terrestrial material is exported to the open ocean (defined here as ocean deeper than 200 m) and how much is retained on continental shelves.

The question of how much riverine material reaches the open ocean is relevant for global biogeochemical budgets and models. Often, global models are too coarse to resolve the comparatively small-scale features of the coastal ocean including individual rivers and their plumes. Riverine inputs to global models are usually represented using an "all or nothing" approach where river inputs are either added directly to the open ocean (ignoring any processing that occurs on the shelf) or ignored altogether. This can be illustrated using the most recent IPCC CMIP5 models summarized in Bopp et al. (2013) and Anav et al. (2013). As shown in Table S1 (see supporting information).

Out of 10 unique models they assessed, only two consider riverine inputs in their ocean model by taking the "all" approach (e.g., Dufresne et al., 2013; Dunne et al., 2013), while the rest assume that there are no riverine inputs to the ocean (e.g., Arora et al., 2011; Ilyina et al., 2013; Moore et al., 2013; Palmer & Totterdell, 2001; Tjiputra et al., 2013; Vichi et al., 2011; Volodin et al., 2010; Watanabe et al., 2011; see also Table S1 in the supporting information).

On a local scale, box models can be useful in assessing export of riverine materials to the open ocean (see, for example, Garvine & Whitney, 2006), but they are difficult to generalize to the global scale. Rabouille et al. (2001) and Laruelle et al. (2009) have attempted to address coastal processing in simple, global mass balance models by assessing coastal ocean nutrient budgets and fluxes. Their approaches consider shelf processing

of materials but do not account for differences between shelf zones around the globe and necessarily make many simplifying assumptions about the physical and biogeochemical processes taking place.

Recently, Sharples et al. (2017) proposed a simple parameterization to describe riverine export to the open ocean based on the ratio of a plume's width (assumed to scale with the internal Rossby radius of deformation) to the local shelf width, which they define as the S_P number. When a plume extends beyond the shelf, Sharples et al. (2017) predict that the material will be exported to the open ocean directly within the plume. Conversely, if the shelf is wider than the plume, no direct cross-shelf transport is expected to occur. This simplified approach holds great potential for providing estimates of retention of riverine material on the shelf versus export to the open ocean. We expand upon the previous work and address a few of its limitations. Specifically, the relationship by Sharples et al. (2017) is based solely on theoretical scaling arguments and uses the S_P number as a binary metric (i.e., export is assumed to be either complete or nonexistent for any given plume) instead of providing a continuous relationship to describe a given plume's export. Here we present a detailed numerical study with the goal of finding empirical parameterizations for cross-shelf and alongshore export, as well as the timescales of export, based on the S_P number and other riverine properties (e.g., discharge).

Our objective is to test the S_P number as a predictor of river plume export through a series of idealized simulations and to develop more descriptive parameterizations of the export. We focus on four influencing factors—latitude, river discharge, winds, and tides—in our simulations and show how they affect plume export of fresh water. The goal is to define simple, general relationships that rely only on easily measured properties of a river (e.g., discharge, latitude, and distance to the shelf break at the river mouth), which can then be applied globally.

2. Methods and Model

2.1. Dynamical Considerations for Model Construction

We are using an idealized numerical model of a river plume and consider a few carefully selected forcing factors. While there are many factors that can influence the dynamics of plumes (see, for example, Horner-Devine et al., 2015), which cannot all be captured in simplified theoretical and idealized approaches, it is useful to study the behavior of plumes under idealized conditions in order to gain insight into the effects and relative importance of individual factors. Furthermore, it is necessary to do so when aiming to derive globally applicable parameterizations.

In an unforced setting, plume dynamics are the result of the underlying behavior of buoyant flows entering the coastal ocean, with latitude and riverine discharge important factors in determining the shape and structure of the plume. At the river mouth, light fresh water encounters denser saline water within an estuary or on the shelf and floats above the ambient water as a buoyant plume. If larger than the Rossby radius of deformation, the plume is influenced by the Earth's rotation through the Coriolis force (Hill, 1998), turning toward the coast in the direction of Kelvin wave propagation (to the right in the Northern Hemisphere and left in the Southern Hemisphere; hereafter referred to as downstream after Garvine, 2001). Two distinct regions are predicted to occur within the resulting plume: an anticyclonically rotating bulge region near the inflow and an alongshore coastal current that remains attached to the coast as it travels downstream. Often, this well-defined theoretical structure is not observed in nature due to complex bathymetry and coastlines and the presence of external forcing factors (e.g., wind and ambient currents), which influence plume structure and transport (Garvine, 2001).

Consideration of a wide range of factors is neither realistic nor desirable where a general description of plumes is sought. Instead, we focus on four primary factors in our analysis: latitude, river discharge, wind forcing, and tides, which are variable around the globe. The first two—latitude and discharge—capture inherent variations among rivers. In addition, we consider winds and tides with the goal of characterizing their impact. The four factors were also the most important in influencing the plume structure during initial numerical tests and can be easily generalized to describe a wide range of plumes (as opposed to, for example, the impact of bathymetry that is more difficult to compare over a wide range of rivers).

Through the Coriolis force, changes in latitude are expected to influence the deflection of the plume, with higher-latitude plumes more likely to remain close to the coast, causing the offshore extent and

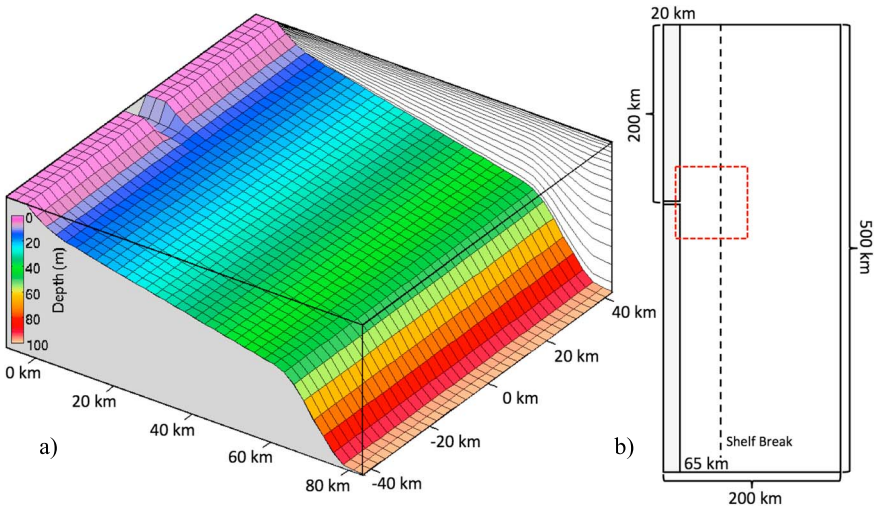

Figure 1. The model domain. (a) A 3D depiction of a subregion of the domain (red box in Figure 1b) with vertical levels indicated by gray lines on the backface. (b) The full domain extends 200 km in the offshore and 500 km in the alongshore direction, with freshwater input to a 5 km wide channel located 200 km from the northern boundary of the domain and 20 km from the coast.

subsequent cross-shelf transport to be small. Overall, discharge and transport are directly related (more water corresponds to more transport); however, high-discharge plumes can also detach from the coast and move offshore (McCreary et al., 1997), which would enhance cross-shelf transport. The presence of tides has been shown to stabilize river plume bulges (Chen, 2014; Isobe, 2005). This is expected to cause a reduction in the offshore extent of the plume, potentially reducing cross-shelf transport.

Winds have the potential to significantly impact plume transport (e.g., Horner-Devine et al., 2015) and are the most complex forcing that we address. Hetland (2005) shows that upwelling-favorable winds can drive a plume offshore, while downwelling-favorable winds force the plume toward the coast. When applied to cross-shelf transport, this suggests that upwelling winds should increase delivery of river-borne materials to the open ocean, with the opposite occurring for downwelling winds. Further, Kourafalou et al. (1996) and Jurisa and Chant (2013) found that plume transport is driven predominantly by wind-induced Ekman transport. Fong and Geyer (2002) note that the response of plumes to wind forcing is much faster than plumes are able to reach a steady state, meaning that the influence of winds strongly determines plume development.

2.2. The Idealized River Plume Model

Our three-dimensional idealized river plume model is implemented using the Regional Ocean Modeling System (ROMS; Haidvogel et al., 2008) in a rectangular domain (Figure 1) covering 200 km in the cross-shore direction and 500 km in the alongshore direction, with 2.5 km horizontal resolution, 15 vertical sigma levels (with tighter spacing near the surface), three open boundaries, and no-slip conditions at the coast. The bathymetry is uniform in the alongshore direction and has a gentle slope of 0.6 m km^{-1} from coast to the shelf break, which is located 65 km offshore. Fresh water enters the domain as a point source (with salinity of 0) through a 10 m deep, 20 km long coastal channel. The ambient salinity is 32, and the water temperature is uniform throughout the domain and identical to the river inflow (no initial stratification). The horizontal extent of the domain, in both the cross-shelf and alongshore directions, is such that none of the simulated plumes interact significantly with the boundaries. Radiation/nudging conditions are prescribed at the open boundaries for temperature, salinity, and 3D momentum, with nudging to the ambient state. A 25 km wide sponge region along the open boundaries, where the viscosity is incrementally increased toward the boundary, further minimizes any boundary interactions. The sponge region was excluded in all subsequent analyses.

The domain was chosen after a series of initial sensitivity tests. These tests showed that the horizontal and vertical resolution is sufficient for resolving many of the plume features and instabilities, without

Table 1
Overview of the Different Model Runs Performed

Latitude	Q ($\times 10^3$ m^3 s^{-1})	Tide	Max. wind (m s^{-1})	Total simulations
DL: Latitude and discharge varied. No tides. No wind forcing				
0°, 1°, 5°, 10°, 15°, 30°, 45°, 60°	1.5, 5, 10, 20, 50, 80, 100	None	None	56
TDL: Same as DL runs but with tidal forcing added				
Same as DL	Same as DL	1 m	None	56
AWDL: Alongshore dominant winds added to DL runs				
Same as DL	Same as DL	None	$u = \pm 1$, $v = \pm 5$	56
XWDL: Cross-shore dominant winds added to DL runs				
Same as DL	Same as DL	None	$u = \pm 5$, $v = \pm 1$	56

significantly limiting computational time (for example, at 1 km resolution there is little change in the simulated plumes, but computation time increases by a factor of 7). Likewise, the simulated plume shape, size, and transport were largely insensitive to the choice of shelf width and slope, except for the high-discharge plumes at high latitudes where bottom advection plays a role in increasing transport. A width of 65 km is wide enough to capture the region where bottom attachment occurs.

The model uses a k–ε turbulence closure scheme, with a background vertical mixing coefficient of 5×10^{-6} m^2 s^{-1}. Initial tests showed that the choice of this coefficient (through doubling and increasing it by an order of magnitude) did not significantly affect the simulated plumes.

We ran the river plume model for the various latitudes, discharges, and forcing scenarios listed in Table 1. On an x86-64 multinode Linux cluster using eight CPUs (two nodes with four CPUs each), each 100 day simulation took approximately 8 h of wall clock time. An internal model time step of 120 s was sufficient for all but the highest-discharge scenarios (100,000 m^3 s^{-1}), for which 60 s was used. The model state was saved every 6 h (although 12 h proved sufficient for capturing most variability) except the tidally forced plumes, which were saved every 3 h in order to avoid aliasing with the 12 h tidal period.

The model was run both with and without forcing from idealized wind and tides (Table 1). For the wind-forced scenarios, we applied a synthetic wind field designed to mimic realistic variability. Actual wind fields from observations were not used in order to maintain generality in the experiments. The idealized wind combines a sinusoidal component that imitates upwelling and downwelling cycles with diurnal on/offshore variability (land sea breeze) and slight random perturbations (Figure 2). For this "realistic" wind scenario, we tested

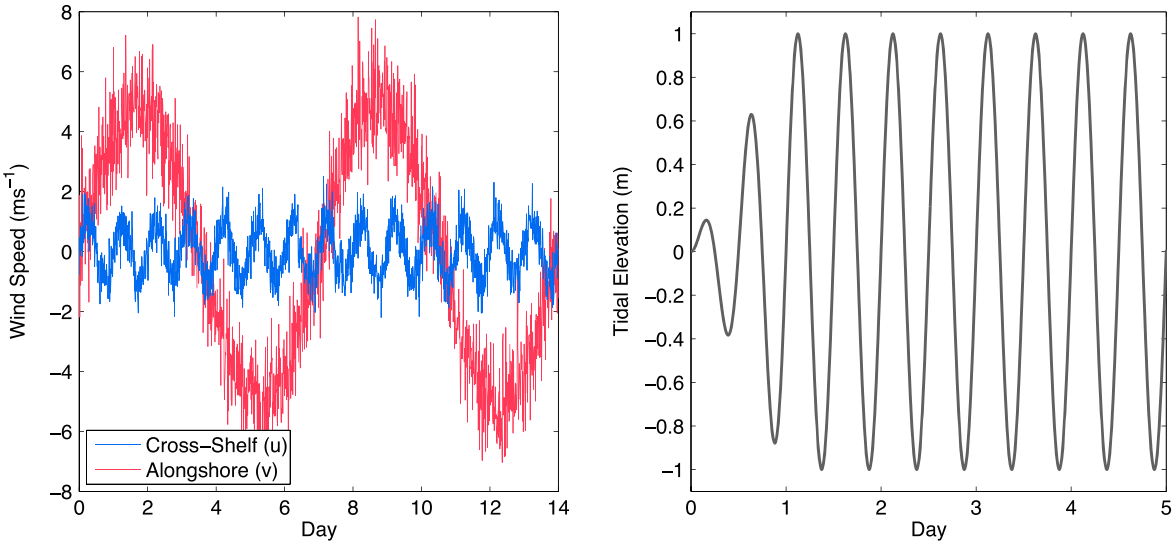

Figure 2. Idealized wind and tidals. (left) The realistic alongshore-dominant wind with a weekly variation between up and downwelling winds (in the alongshore direction), superimposed by a weaker diurnal land/sea breeze (cross-shore). (right) The 12 h tidal signal applied to the domain was ramped up over the first day.

the influence of direction with two different wind fields: one where the alongshore component is stronger (with a maximum wind speed of 5 m s^{-1} alongshore and 1 m s^{-1} cross-shore) and one where the cross-shore on/offshore variability is stronger (maximum speed of 5 m s^{-1} cross-shore and 1 m s^{-1} alongshore). Wind is applied uniformly throughout the entire domain over the complete duration of the simulations, converting wind speed to wind stress using a drag coefficient of 1.25×10^{-3} (Kara et al., 2007).

For the tidally forced model runs, we applied a 12 h (semidiurnal) tidal cycle at the eastern boundary, such that the elevation at the coast is 1 m (Figure 2) and the imposed tidal currents are 0.1 m s^{-1}. This tidal forcing is, of course, highly idealized when compared to tides around the world. However, it allows us to assess the influence of changes on a tidal timescale in a simple manner. To avoid numerical instabilities, the tides ramped up to their maximum elevation over the course of 1 day. The model state was saved at the peak tidal amplitudes (1 m), as well as the maximum ebb/flood conditions (at the inflection points of the sinusoidal wave).

2.3. Metrics Used to Assess Simulated Plumes

Our analysis focuses on just two primary metrics: the S_P number proposed by Sharples et al. (2017) and the export efficiency. These metrics are easily calculated from numerical model output and use simple and easily accessible characteristics of plume properties, such as river discharge, as input parameters.

2.3.1. The S_P Number

Sharples et al. (2017) use the S_P number to relate the approximate width of a plume (estimated as 4.3 times the internal Rossby radius: $4.3Ro'$) to the local shelf width (W_S):

$$S_P = \frac{4.3R_o'}{W_S} \tag{1}$$

When $S_P > 1$, as might occur for low-latitude plumes where Ro' is large, or at active margins where the shelf width is small, Sharples et al. (2017) assume that river-borne materials are efficiently transported to the open ocean. Conversely, a value of $S_P < 1$ indicates that direct transport to the open ocean is negligible. Other studies have shown that the width of the plume can vary in relation to the Rossby radius depending on the forcing conditions (e.g., Yankovsky & Chapman, 1997), but the factor of 4.3 is used here to maintain consistency with the analysis performed by Sharples et al. (2017). The Rossby radius is the length scale over which the Earth's rotation becomes important for influencing fluid motion and can be defined mathematically as follows (Csanady, 1971):

$$R_o' = \frac{\sqrt{\frac{g}{\rho_o}\Delta\rho h}}{f} \tag{2}$$

where g is the acceleration due to gravity, ρ_o is the ambient density (here 1,025 kg m^{-3}), $\Delta\rho$ is the anomaly between the mean plume density and the ambient density, h is the mean plume depth, and f is the Coriolis parameter (which depends on the sine of the latitude).

2.3.2. Export Efficiency

Export efficiency, $E_D{}^M$, is defined here simply as the ratio of the total, time-integrated cross-shelf transport, $\Gamma_D{}^M$, where D refers to either the cross-shelf or along-shelf direction (X or A, respectively) and M to the material being transported (e.g., fresh water or nutrients) divided by the total, time-integrated river input/load of the component, L^M_{River} (discharge, Q, is used in the case of fresh water). Export efficiency thus provides a measure of the fraction of river-borne materials being exported either in the cross-shelf direction to the open ocean or downstream from the source in the coastal current:

$$E_D^M = \Gamma_D^M / L^M_{\text{River}} \tag{3}$$

It then follows that the fraction of material exported across the shelf ($E_X{}^M$) and the amount of material retained on the shelf ($R^M{}_{\text{Shelf}}$), which can be further broken down into near source retention ($R^M{}_{\text{Source}}$) and far-field alongshore export in the coastal current ($E_A{}^M$), is equal to 1:

$$\begin{aligned} 1 - E_X^M &= R^M_{\text{Shelf}} \\ &= R^M_{\text{Source}} + E_A^M \end{aligned} \tag{4}$$

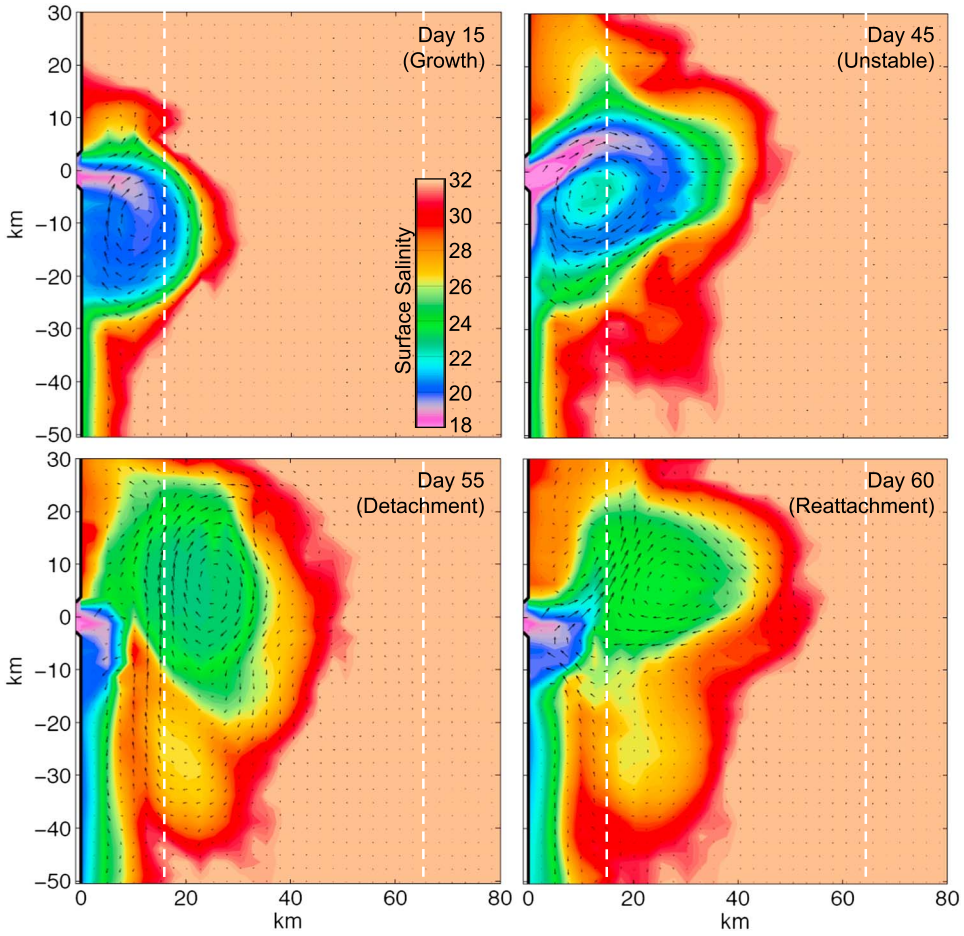

Figure 3. Snapshots of plume evolution at 45° for a discharge of 1,500 m^3 s^{-1} illustrating different stages of bulge development. The white dashed lines show the 15 km and 65 km transects where freshwater transport is calculated. (from top left to bottom right) Initial growth of the bulge and establishment of the downstream coastal current (<20 days), the plume becomes unstable (> 30 days), the unstable bugle detaches around day 55, and the bulge reattaches around day 60.

The transport of a material is calculated as the net flux through a plane at a constant distance either from the coast in the cross-shelf direction or from the river mouth in the alongshore direction (e.g., Fong & Geyer, 2002). The net cross-shelf freshwater transport is as follows:

$$\Gamma_X^{FW} = \sum_{y,z} F_{FW}(x,y,z) \cdot u(x,y,z) \Delta y \Delta z(x,z) \tag{5}$$

where u is the cross-shelf velocity at each grid cell. The alongshore transport is calculated analogously. F_{FW} is the "freshwater fraction" (analogous to a concentration of fresh water; following Lehrter et al., 2013), a measure of the proportion of river water (salinity of 0) within a given parcel or grid cell, calculated as follows:

$$F_{FW} = \frac{S_0 - S}{S_0} \tag{6}$$

S is the salinity of the parcel/grid cell, and S_0 is the ambient salinity (here 32). Export efficiency is easy to calculate from a numerical simulation but much harder (if not impossible) to obtain in the field. In order to use equation (5) to estimate nutrient export, F_{FW} has to be replaced by the nutrient concentration of the plume water (in kg m^{-3}). Nutrients are not explicitly considered here. In part 2 of this paper (Izett & Fennel, 2018), nutrient export is estimated, and the role of different export timescales in determining the overall nutrient export for different rivers is considered in detail.

We calculated cross-shelf freshwater transport both at a nearshore location (15 km; just wide enough to exclude the coastal current in each of the simulated plumes) and at the model shelf break (65 km), as well as the alongshore transport at 150 km downstream of the river mouth, which is both well outside the bulge region and also uninfluenced by the boundary of the domain (see Figure 1).

3. Results

3.1. Idealized Model Experiments

We ran the idealized river plume model for 100 days with a range of forcing scenarios as described in Table 1 in order to assess the impact of different factors on plume export. Below 5°, the simulated plumes do not form a coastal current due to the weak Coriolis force. Instead, they spread offshore from the inflow in a near symmetric, non-rotational plume. At latitudes 5° and above, a bulge forms at the river mouth, and the plume is deflected forming the expected downstream coastal current (Figure 3). The bulge is smaller for higher-latitude plumes and more spread out at low latitudes. The addition of tides causes only slight onshore and offshore motion of the plume with the tidal ebb and flood (Figures 4a/4g and 4b/4h). Winds either force the plume offshore during upwelling conditions or, under downwelling conditions, suppress the plume and enhance the coastal current (Figures 4c–4f/4i–4l).

Most of the simulated plumes remain near the surface, detaching from the bottom close to shore and reaching less than 10 m in mean depth. Only the high-discharge plumes (at $>$50,000 $m^3\ s^{-1}$) penetrate deep enough to interact with the bottom over significant distances. At high latitudes, the highest-discharge plumes (80,000 $m^3\ s^{-1}$ and 100,000 $m^3\ s^{-1}$) remain attached almost out to the domain shelf break at 65 km offshore.

In all cases, the plume grows initially and evolves continuously in time; however, cross-shelf transport reaches an approximately constant mean value after no more than 20 days. During the constant-transport phase, the freshwater export varies about a mean value due to instabilities that develop along the plume front, which vary depending on latitude, discharge, and external forcing. For all simulated plumes above 5°, the entire bulge eventually becomes unstable, causing it to detach and reattach on varying timescales. High-latitude and high-discharge plumes are much less stable than those at lower latitudes and for small discharges and have overall more dynamic bulge regions. All of the results presented here are after the initial 20 day development period, that is, during the phase of approximately constant mean transport when the plume is established. The total export is calculated using equation (5) over the remaining 20–100 days, with the export efficiency determined as the net export over the entire 80 day period, divided by the total riverine discharge over that time (equation (3)). By calculating over such a long integration period, we average out bulge recirculation over smaller time periods.

In all simulations, cross-shelf export efficiency is larger for higher discharges and lower latitudes but decreases with increasing latitude (the opposite is true for the alongshore export; Figure 5). At a constant discharge, E_X^{FW} decreases with increasing latitude from close to 100% efficiency near the equator to almost no transport at high latitudes. Conversely, cross-shelf export efficiency increases with increasing discharge by as much as 30% between the lowest-discharge case (1,500 $m^3\ s^{-1}$) and the highest-discharge case (100,000 $m^3\ s^{-1}$). Low-latitude and high-discharge plumes are much more efficient exporters than high-latitude, low-discharge plumes.

Across all discharge scenarios, the efficiency of simulated cross-shelf export for the plumes at or above 30° latitude is less than 65% beyond 15 km from the shore and less than 50% beyond 65 km from the shore. Without any external forcing from wind or tides, low-discharge plumes (10,000 $m^3\ s^{-1}$ or less) at high latitudes have a very low cross-shelf export efficiency (less than 5% beyond 65 km above 45°). Tidal forcing reduces the overall transport beyond 65 km offshore, but the wind forcing is able to overcome some of the influence of latitude and increases transport at higher latitudes due to the influence of wind-induced Ekman transport. The low-discharge plumes have similar export efficiencies as the high-discharge plumes under wind-forced conditions. For both the wind-forced and tidally forced simulations, the lower-discharge plumes are more affected by the added forcing than the higher-discharge plumes, especially at the lower latitudes. Overall, wind forcing has a greater impact on the simulated plumes than tidal forcing.

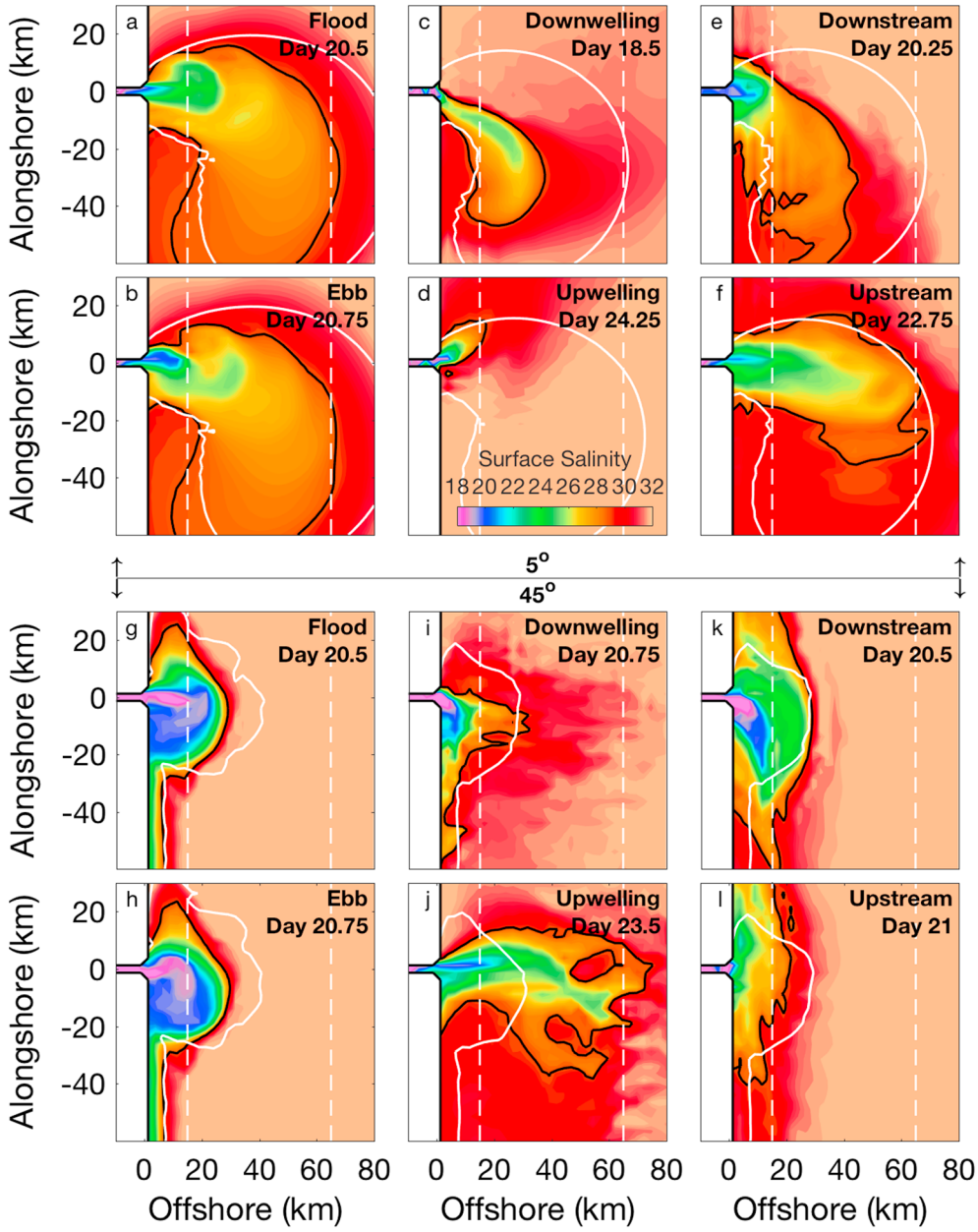

Figure 4. Simulated plumes after 20 days under different forcing conditions at 5° and 45° latitude for a discharge of 1,500 $m^3\ s^{-1}$. The white dashed lines show the 15 km and 65 km transects where freshwater transport is calculated. (a/g and b/h) At ebb and flood tide (TDL scenario); (c/i and d/j) under downwelling- and upwelling-favorable winds (AWDL scenarios); (e/k and f/l) under on/offshore wind cycle in the cross-shelf-dominant wind forcing (XWDL). The 29-salinity contour is shown in black. The same salinity contour from the unforced simulation (Figure 3) is also shown (white line) for comparison.

It should be noted that the idealized wind forcing is symmetric (Figure 2), with both upwelling and downwelling components. As such, the overall export efficiency we calculate between days 20 and 100 of the simulations is the mean value of an oscillatory signal. Figure 6 shows that on a shorter timescale (e.g., a few days), the specific wind field has a much greater influence on the plumes than over the longer timescale where the latitude-dependent influence of the Coriolis force is dominant. In this case, export is either significantly enhanced due to upwelling or significantly reduced due to downwelling, with the freshwater being alternately driven offshore and back onshore.

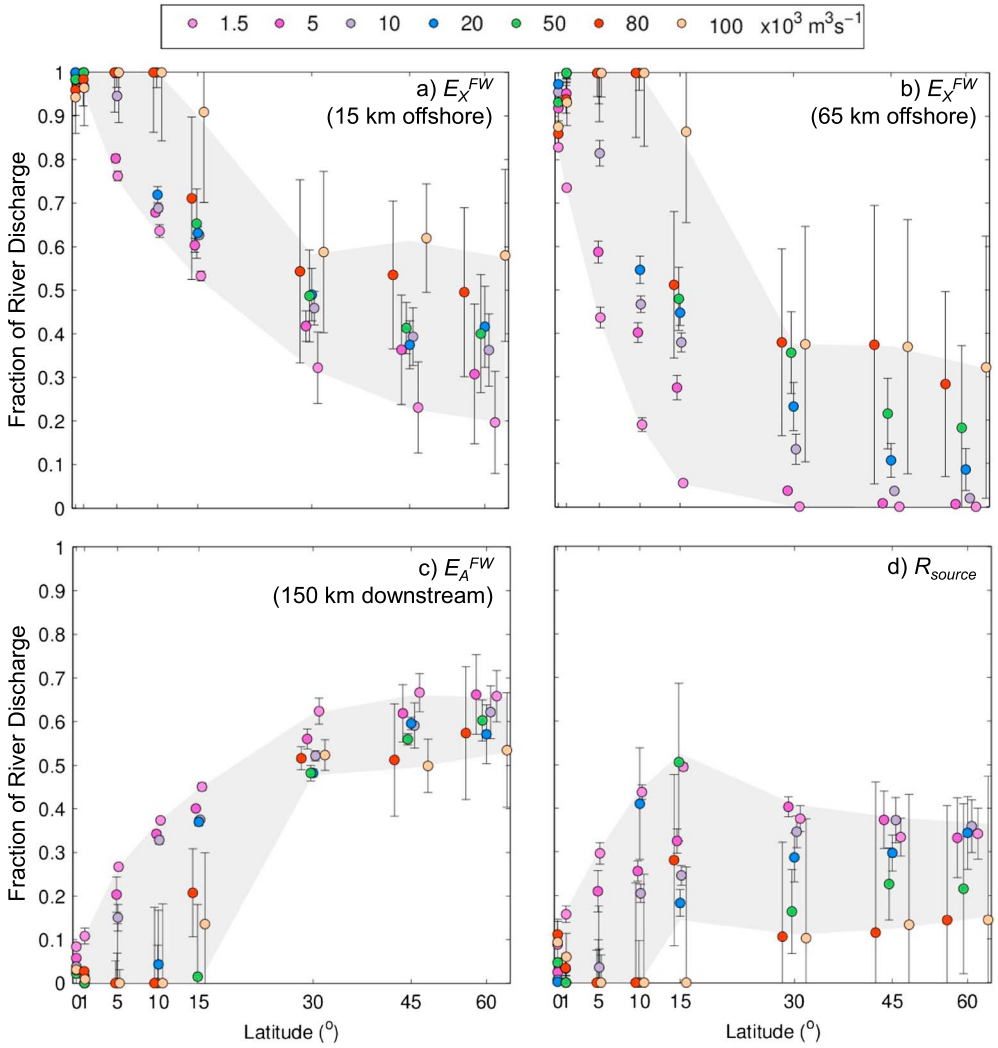

Figure 5. Simulated export efficiency and shelf retention of fresh water as a function of latitude for all discharge scenarios (colored markers) without any forcing from wind or tides (DL; Table 1). The gray shading shows the maximum and minimum range of the data. (a) Cross-shelf export efficiency past 15 km and (b) past 65 km. (c) Alongshore export in the coastal current. (d) Retention near the source. The data are slightly offset from their respective latitudes (by up to ±2%) in order to distinguish overlapping data. For the other forcing scenarios listed in Table 1, please see supporting information Figures S1–S3.

Plumes that are attached to the bottom further offshore have greater export efficiencies than plumes that detach closer to the coast at the same latitude. The purely surface-advected plumes (for lower discharges) have similar export efficiencies, while the bottom-attached plumes (for higher discharges) have up to 30% higher export efficiency (for example, the 80,000 and 100,000 $m^3\ s^{-1}$ plumes in Figure 5).

The simulated alongshore freshwater export efficiency, E_A^{FW}, follows a trend that is opposite to the cross-shelf export efficiency. At low latitudes, the alongshore transport is close to zero for all discharges, with increasing export efficiency toward higher latitudes. The lower-discharge plumes have greater alongshore export efficiency than the high-discharge plumes. At high latitudes, the alongshore export efficiency is between 55% and 70%. Overall, the amount of fresh water retained near the source is just 0–40%, with higher retention at higher latitudes and lower discharges.

3.2. Simple Relationships for Predicting Plume Export

Building on Sharples et al. (2017), the goal of this research is to test the validity of estimating cross-shelf plume transport using simple descriptors of the plume (such as the S_P ratio) and determine empirical

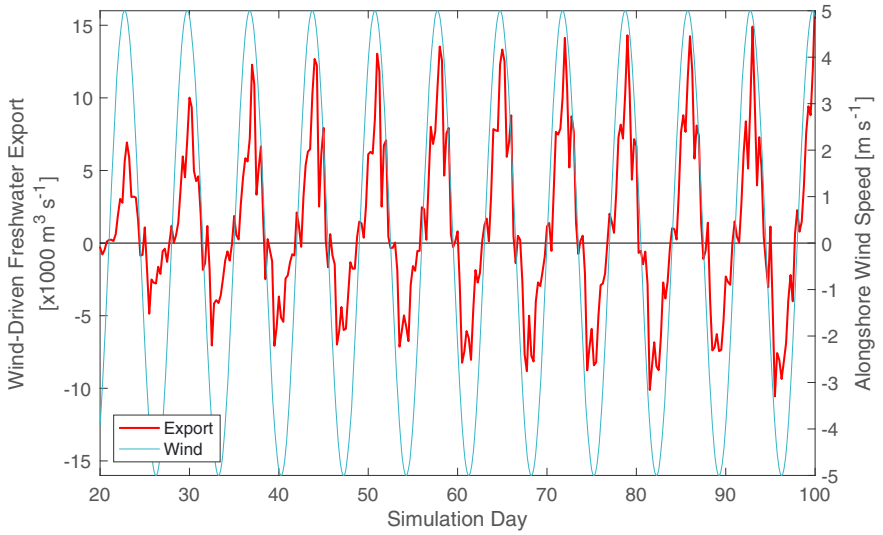

Figure 6. Wind-driven freshwater export with the unforced export subtracted for the AWDL simulation at 45° and a discharge of 5,000 m^3 s^{-1} compared to the alongshore wind speed.

relationships that can be used to parameterize plume export. To this end, the following presents relationships derived through applying a series of regressions to the simulated data. We ensure no unrealistic values are predicted by the regressions (e.g., export no greater than 100%), but otherwise, they are statistical best fits, rather than physical derivations. One of our aims was to assess how well the S_P number predicts cross-shelf river plume export. Comparing the export efficiency of the simulated plumes at 15 km and 65 km offshore to their S_P number (Figure 7a), the simple application of an S_P = 1 threshold as presented by Sharples et al. (2017) is far too simplistic when compared to the idealized model results. While the behavior is qualitatively different above and below S_P = 1, the simulated export is continuous in its distribution, with a fraction of fresh water being delivered across the shelf even for very small S_P. We used regression analysis to fit an asymptotic function of the following form:

$$E^{FW} = \frac{\zeta - 1}{\zeta} \tag{7}$$

where $\zeta = aS_P^{1/2} + b$.

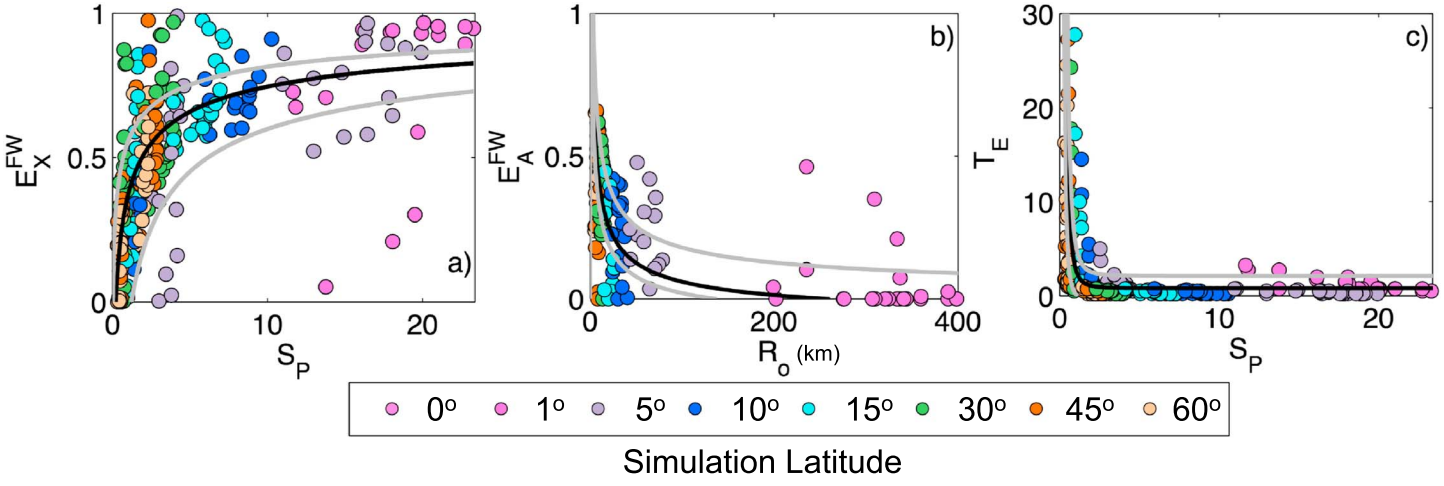

Figure 7. Regressions of simulated export parameters for all latitudes. (a) E_X^{FW} as a function of S_P (equation (7)), (b) E_A^{FW} as a function of Ro' (equation (8)), and (c) T_E as a function of S_P (equation (9)). See Table 2 for the regression coefficients.

Table 2
Regression Coefficients for Each of the Idealized Relationships Presented in Section 3.2

Equation	a	b	r^2	Figure
E_X^{FW} (equation (7))	1.1 ± 0.4	0.5 ± 0.3	0.77	Figure 7a
E_A^{FW} (equation (8))	1.6 ± 0.2	−0.10 ± 0.02	0.53	Figure 7b
T_E (equation (9))	0.2 ± 0.1	0.8 ± 1.3	0.72	Figure 7c
$\Delta\rho h$ (equation (10))	70 ± 6	43 ± 5	0.95	Figure 8b

The functional form was chosen to ensure that export efficiency approaches but never exceeds 100% as S_P increases. Other empirical forms were tested, but a 1/2 dependence on S_P as above provides the best fit. In order to avoid unrealistic values in the regression, b is bounded by 0 and 1, and $a > 0$. Where S_P values are below the x intercept of $((1 - b)/a)^2$, all estimates should be set to 0 (non-negative E_X). The values of the coefficients a and b as obtained from the numerical simulations are listed in Table 2.

The asymptotic regression predicts cross-shelf export efficiency very well from the plumes' S_P number in most of the simulations, with a regression applied to the entire data set (all forcing scenarios combined) to obtain a means of estimating export under a range of forcing scenarios (Figure 7a). The uncertainty ranges for the regression capture roughly 80% of the data points. Table 2 lists the regression coefficients in equation (8) and their uncertainties (95% confidence intervals). The fit is limited, however, if only applied to the midlatitudes where the influence of wind and tides increases transport above the curve or only to low latitudes (large S_P) where the influence of the Coriolis force is negligible, and the role of winds, tides, and overall discharge are more important in determining the ultimate export.

Other plume properties can also be estimated using simple relationships. The simulated alongshore freshwater export efficiency (E_A^{FW}) 150 km downstream from the river mouth, for example, should depend on the latitude (increasing latitude leads to greater transport in the coastal current with increased deflection of the plume by the Coriolis force). An $Ro^{-1/2}$ dependence results in the best fit to the simulated exports (Figure 7b):

$$E_A^{FW} = aRo'^{-1/2} + b \tag{8}$$

The regression is not as strong as the one for the cross-shelf export, with an r^2 value of just 0.53, but it does provide a rough estimate of the corresponding alongshore export compared to the cross-shelf export. This equation can result in estimates of E_A^{FW} that are greater than 1 (for small Ro'), and when used with equation (7), it is possible that $E_A + E_X$ could be greater than 1. Of course, this is not physically possible, so all estimates for real rivers should be constrained such that $0 \le E_A \le 1 - E_X$.

As with cross-shelf export, we found that the S_P number can be used to predict the export timescale (T_E) of the simulated plumes (the time it takes for the plume to first reach the shelf break). This is an important parameter when considering the uptake of nutrients on the shelf, with the lifetime of plumes determining how long the nutrients are available to be consumed before export to the open ocean. In the numerical experiments, T_E scales as linearly proportional to S_P^{-3} (Figure 7c),

$$T_E = aS_P^{-3} + b \tag{9}$$

with an r^2 value of 0.72. As with the estimation of the alongshore export efficiency, this relationship can also predict negative T_E values for large values of S_P when estimated using the 95% confidence intervals for the regression. To avoid this, all negative values should be set to zero when using the relationship to estimate nutrient processing for real rivers.

Each of the above relationships requires knowledge of the Rossby radius of a plume, which is difficult to estimate. From equation (2), the Rossby radius depends on the product: $\Delta\rho h$, where $\Delta\rho$ is the density anomaly between the plume and ambient water and h is the mean depth of the plume. While the other parameters are easily obtained (such as the latitude), $\Delta\rho$ and h are difficult, if not impossible, to measure in field studies of real plumes. Sharples et al. (2017) estimate the numerator of equation (2) as the mean value from 20 rivers around the world such that the estimated Rossby radius only depends on the Coriolis parameter. However, our numerical simulations show that the Rossby radius also has a strong dependence on discharge. Thus, we sought to estimate the numerator with an

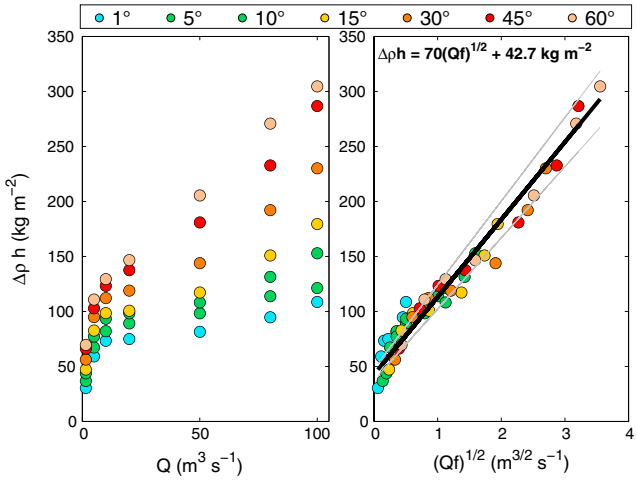

Figure 8. $\Delta\rho h$ as a function of discharge and latitude. (a) $\Delta\rho h$ as a function of discharge alone. (b) $\Delta\rho h$ as a function of both discharge and latitude.

empirical relationship to determine $\Delta\rho h$ (the other terms are constants). Applying a linear regression to river discharge (Q) alone, $\Delta\rho h$ increases approximately linearly with discharge for our simulated plumes (r^2 of 0.67); however, a strong dependence on latitude remains (Figure 8a). Hence, we looked for a relationship with dependence on both the discharge and the Coriolis parameter (f). Based on physical scaling arguments relating the volume of the plume to the discharge, the product should depend on $(Qf)^{1/2}$, which leads to a very good linear fit (Figure 8b):

$$\Delta\rho h = a\sqrt{Qf} + b \tag{10}$$

By including the latitude dependence, the goodness of fit increases significantly, resulting in an r^2 value of 0.95.

Table 2 lists the coefficients for each of the relationships found through applying regressions to the simulated model output.

4. Discussion

4.1. Idealized Model Experiments

We conducted a series of idealized model experiments to assess the influence of four primary factors on cross-shelf transport of river water in plumes. The four factors are latitude, river discharge, tidal forcing, and wind forcing.

In general, the simulated plumes form and behave as predicted by theory (see, for example, Horner-Devine et al., 2015, for a more detailed overview). At latitudes 5° and above, the buoyant outflow at the river mouth is deflected by the Coriolis force, resulting in the formation of a bulge and coastal current (Figure 3). With increasing latitude, this downstream deflection intensifies, and the plumes become deeper at higher latitudes and for higher discharges. Without any external forcing beyond latitude and discharge, this classical shape persists for the duration of the simulations; however, when external forcing is applied, the shape of the simulated plumes changes and plumes can be pushed offshore or onshore depending on the forcing.

All of the simulated plumes—forced and unforced—reach a point of approximately constant cross-shelf transport at or before 20 days of simulation time; however, the bulge never completely stabilizes to a steady-state shape and size. In the unforced case, this is the result of continuous growth of the bulge region (as discussed by Garvine, 2001), while the dynamic nature of the plumes in the forced scenarios leads to continual reshaping of the plumes. Overall, the simulated plumes for high-discharge and low-latitude cases extend further across the shelf than those for low-discharge and high-latitude cases. In order to assess a mean transport and avoid the plume growth period in our analysis, we calculate the export between 20 and 100 days.

The main pathway for cross-shelf export within the simulated plumes is through direct advection within the bulge region (as opposed to downstream where transport is more diffuse and indirect). This occurs in two ways: (1) through cross-shelf growth and advection of the plume, and (2) through the development of instabilities along the front demarcating the plume. In the absence of external forcing, the continuous growth of the bulge region carries riverine water offshore. In all of the unforced cases, the initial bulge eventually grows so large that it becomes unstable and detaches from the rest of the plume before recirculating and eventually reattaching on different timescales depending on the latitude and discharge of the plumes (Figure 3). Such large-scale instabilities are described by Oey and Mellor (1992). Similarly, smaller instabilities develop along the plume front, enhancing cross-shelf transport via offshore movement of the resulting eddies.

In all simulations, latitude provides a strong control on the efficiency of cross-shelf transport. With increasing latitude, the cross-shelf export decreases significantly, with the greatest decrease in transport occurring for the unforced case (approximately 70% from 0° to 60°). Correspondingly, as the cross-shelf transport decreases with increasing latitude, the alongshore transport within the coastal current increases, while the near source retention remains approximately constant above 5° at roughly 30%.

Increasing discharge has a slightly nonlinear effect on plume transport. In most simulations, export efficiencies at low discharges are similar; however, the higher-discharge simulations are more spread out, resulting in as much as a 30% change between the lowest and highest transport values at 60° for the unforced simulations. It is apparent that the greater cross-shelf transport efficiency for high discharges (and subsequently

reduced alongshore transport efficiencies) is consistent with the process of bottom advection as described, for example, by Yankovsky and Chapman (1997). The plumes that are entirely surface advected are generally similar in their export efficiencies. However, the plumes that are attached to the bottom much further offshore (i.e., the higher-discharge cases) have higher cross-shelf transport efficiencies than the surface-advected plumes and lower alongshore transport efficiencies. At 45° in the unforced simulations, for example, the plumes with discharges less than 10,000 $m^3\ s^{-1}$ are all surface-advected, and cross-shelf transport is less than 5% beyond 65 km for all of them (Figure 5b). The plumes with discharges above 20,000 $m^3\ s^{-1}$ are all attached to the bottom to at least 10 km from the coast and have correspondingly increased cross-shelf transport: all the way up to the 100,000 $m^3\ s^{-1}$ plume, which reaches almost to the shelf break after 20 days and has an export efficiency of almost 40%. The impact of bottom advection is greater at higher latitudes due to deepening of the plume but is less noticeable for the forced plumes than the unforced plumes, where the external forcing exerts greater control over the plume dynamics.

Overall, the wind-forced scenarios (XWDL and AWDL) have the highest cross-shelf export efficiencies of all the simulations, increasing cross-shelf export efficiency by up to 70% compared to the base case and overcoming some of the influence of latitude (see Figures S2 and S3 in the supporting information). However, in all of the model experiments, cross-shelf transport still decreases with latitude (by as much as 70% in the unforced case and 50% with wind forcing between 0° and 60°). Consistent with Sharples et al. (2017), the fact that the Coriolis force exerts a strong control in all cases suggests that it is the main factor determining whether river-borne materials are exported to the open ocean, reducing the offshore extent of river plumes and subsequent cross-shelf transport. External forcing from wind and tides is only able to overcome some of the overriding influence of the Coriolis force. It does, however, lead to an increase in the amount of cross-shelf transport that occurs outside the bulge region due to advection of the plume. While beyond the scope of this study, it would be useful to quantify the proportion of near-source versus far-field cross-shelf transport.

4.2. Simple Relationships Predicting Plume Export

One of the objectives of this research is to test the validity of using simple metrics—such as the S_P number proposed by Sharples et al. (2017)—to describe river plumes, in particular their associated open ocean export. Despite the variability of the simulated plumes under different influencing factors, clear relationships emerge between simple plume descriptors and properties of the simulated plumes.

We find that the alongshore export efficiency of the simulated plumes can be related to the inverse of the square root of the Rossby radius (Figure 7b; equation (8)). Previously, Fong and Geyer (2002) demonstrate the relationship between alongshore export and the Rossby number (riverine discharge velocity divided by the product of the Coriolis parameter and the width of the river mouth). This was followed by Horner-Devine et al. (2006) who present a simple relationship to describe export as a function of the Rossby number using rotating-tank experiments. However, their results are for a much smaller range of Rossby number than we include here and do not consider external forcing. Similarly, in a numerical setting, the Rossby number is relatively easy to define; however, for a real-world river system, where the inflow can be a diffuse source (such as an estuary), the Rossby number becomes more difficult to define. For a single river system, this is perhaps not too great an obstacle to overcome, but in the context of obtaining a global, general estimate of riverine export, the need to obtain information about thousands of rivers makes this approach intractable and hence our empirical approach using the Rossby radius.

The Rossby radius, which depends on latitude through the inverse of the Coriolis parameter (equation (2)), also provides an indication of a plume's ability to spread offshore. The higher the latitude, the stronger the Coriolis force, resulting in greater downstream deflection of the plume and correspondingly increased transport in the coastal current and decreased cross-shelf transport.

Similarly, we find that the S_P number (equation (1)) predicts the cross-shelf export efficiency very well through a simple asymptotic relationship (equation (7)). As discussed by Sharples et al. (2017), cross-shelf export efficiency is qualitatively different for plumes with an S_P number less or greater than 1. However, whereas Sharples et al. (2017) assume complete export for $S_P > 1$ and no direct export for $S_P < 1$, we estimate the export using a continuous function (Figure 7a; equation (7)). For $S_P < 1$, the export efficiency is low but increases rapidly with increasing S_P. Above 1, the overall export efficiency is higher, but the rate of

increase in export efficiency with increasing S_P is much lower as the curve levels off. It is important to note that the regression has a positive x intercept. This indicates that plumes below a given S_P number do not directly export material to the open ocean. The confidence intervals on the estimates cover just over 80% of the simulated estimates, which indicates that the regressions are reliable for estimating export in more complex forcing environments. To further improve the estimates, an obvious next step would be to refine the relationships with more realistic plume models and to assess how they apply under the influence of more complex forcing scenarios, but this is beyond the scope of the present study.

The globally applicable relationships (Figures 7a and 7b) are derived empirically and strongly influenced by low-latitude rivers (high S_P and Ro'), which lead to the sharp curvature. If low-latitude rivers were excluded from the analysis, the relationships would be very different: more linear and potentially with a larger spread in the coefficients due to the influence of winds and tides at these latitudes.

Also important in calculating export in real rivers is the time the plume remains on the shelf. The longer water remains on the shelf before being exported, the greater the potential for nutrients to be processed and transformed into forms less likely to be exported. Figure 7c shows that the export timescale for all of the simulated plumes (calculated as the time before cross-shelf transport first occurs) can be estimated as a linear function of S_P^{-3} (equation (9)). Intuitively, this makes sense: a larger S_P number means either a large plume, or a small shelf, such that cross-shelf export is direct and efficient (and the export timescale short). Smaller S_P, on the other hand, indicates a small plume in relation to the shelf, with export taking much longer. This has significant implications for the control of the S_P number on nutrient export. Not only do small S_P plumes export less riverine material compared to larger S_P plumes (equation (5)), they also do so on a much longer timescale with greater nutrient depletion before export. The role of the export timescale, and different shelf processing rates, is addressed in greater detail in part 2 of this study (Izett & Fennel, 2018).

These relationships all describe export as a function of the Rossby radius (the S_P number is calculated with Ro' in the numerator) and can be used to estimate export for real rivers. This, of course, requires knowledge of the Rossby radius for real plumes, which is not always straightforward. In equation (2), the Rossby radius depends on the product $\Delta\rho h$, which is difficult to measure for real plumes, even in dedicated field studies ($\Delta\rho$ is the density difference between the plume and ambient water, and h is the mean plume depth). Sharples et al. (2017) estimate this using a global mean value from measurements of 20 real world plumes. However, our simulations show an apparent dependence on both latitude and discharge, so we apply a regression to our simulation results that relates $\Delta\rho h$ to the river discharge and the Coriolis parameter (equation (10) and Figure 8b). The regression provides an extremely good fit for the simulated plumes (r^2 of 0.95) and as such is assumed to be a good predictor for real world plumes as well, making it easy to estimate the Rossby radius of a real plume.

Extending the work by Sharples et al. (2017), we use a continuous relationship to describe river plume export as a function of the S_P number, as opposed to a threshold value of $S_P = 1$. We further propose to define the S_P number as simply the dimensionless ratio of the Rossby Radius to the shelf width, rather than being multiplied by a constant coefficient. The use of a continuous function inherently absorbs the coefficient into the regression coefficients and therefore eliminates the discussion surrounding the "true" value of the plume width, which is fluid and poorly defined in the natural environment.

It should be noted that the forcing used here is idealized compared to the forcing in real-world systems. In reality, the plume environment can change on various timescales, including seasonally (e.g., changes in thermal stratification or wind fields). The environment of every plume is unique and highly variable, with other factors not addressed here (such as ambient currents, complex coastlines, and bathymetry) influencing offshore export. This is particularly true for the influence of wind on plume export. From Figure 6, for example, a midlatitude plume with sustained upwelling winds would have significantly more cross-shelf export than a midlatitude plume with sustained downwelling winds. However, for the purpose of this research, where our goal is to obtain a general description of plume behavior, the simplifications presented here help to elucidate the underlying influences that can affect plumes, while the uncertainty range in regression coefficients captures some of the unexplained variability due to factors that have not been addressed here.

The main result presented here is a demonstration that plume dynamics, despite their complexity, can be described using simple relationships, at least to a first-order approximation. Given the complex nature of

the different forcings that can influence plumes, we would expect that the simplified relationships do not apply for all situations; however, the fact that the simple relationships apply for most of the idealized scenarios builds confidence that reasonable estimates of plume transport can be obtained through this framework. Our results support the use of the S_P number proposed by Sharples et al. (2017) to predict cross-shelf plume export, while at the same time extending their work by parameterizing not only the cross-shelf export but the alongshore export and export timescale as well, in terms of continuous functions derived from numerical model output. Overall, these relationships allow for the easy estimation of plume export for real-world plumes, by first calculating the Rossby radius, and subsequently the cross-shelf and alongshore transport within the plumes. From these simple estimates, budgets of freshwater and nutrient transport can be calculated for any river. These are presented in part 2 of this study (Izett & Fennel, 2018).

5. Conclusions

We conducted a series of idealized model experiments to assess the impact of different factors on the export of terrestrially derived materials within river plumes to the open ocean. Latitude is the dominant controlling factor in determining the efficiency with which cross-shelf export occurs. At higher latitudes, where the Coriolis force is strong, deflection of the plume results in increased alongshore transport and significantly reduced cross-shelf export. Simple, latitude-dependent metrics can be used to estimate plume transport across a range of different forcing scenarios. In particular, we show that the cross-shelf export of riverine material is predicted by the S_P number of a plume as proposed by Sharples et al. (2017) through a simple asymptotic relationship, allowing for easy estimation of export for real plumes.

By using an idealized model, various factors were explored in isolation, allowing for a general description that can be applied to a wide range of settings. The derived relationships between S_P and export can be used to estimate riverine export for any river, with just a few easily obtainable parameters (such as discharge) needed to be known. The integration of such estimates into global models is straightforward.

This work represents the first numerical exploration of a general relationship to describe cross-shelf export, following the theoretical arguments of Sharples et al. (2017). Future work should explore the S_P number in more complex scenarios, including in specific regional models of river systems. This would enable further understanding of where the relationships are valid and under what conditions they break down beyond the idealized test cases presented here. Such conditions could be regions of complex bathymetry, complex shelf dynamics, or with variable forcing.

In part 2 of this study (Izett & Fennel, 2018), we apply the relationships developed herein to estimate the export of fresh water and nutrients for real rivers across the globe.

Acknowledgments

We are grateful to Jonathan Sharples for his willingness to share and discuss his results throughout the preparation and completion of this research. We also thank Rachel Horwitz, Jinyu Sheng, Chris Algar, and Michael Whitney for comments on an early draft of this manuscript and Alex Horner-Devine and one anonymous reviewer for their constructive comments. The simulations were performed using the open-access ROMS, which is freely available (https://www.myroms.org) and should be reproducible with the information described in the manuscript. The supporting information contains simulation data and derived values used to obtain the relationships described herein (Tables S1 and S2). J.I. was funded through the NSERC CGS-M award and the Nova Scotia Scholarship. K.F. acknowledges funding from the NSERC Discovery Program.

References

Anav, A., Friedlingstein, P., Kidston, M., Bopp, L., Ciais, P., Cox, P., … Zhu, Z. (2013). Evaluating the land and ocean components of the global carbon cycle in the CMIP5 Earth system models. *Journal of Climate*, *26*(18), 6801–6843. https://doi.org/10.1175/JCLI-D-12-00417.1

Arora, V. K., Scinocca, J. F., Boer, G. J., Christian, J. R., Denman, K. L., Flato, G. M., … Merryfield, W. J. (2011). Carbon emission limits required to satisfy future representative concentration pathways of greenhouse gasses. *Geophysical Research Letters*, *38*, L05805. https://doi.org/10.1029/2010GL046270

Bentsen, M., Bethke, I., Debernard, J. B., Iversen, T., Kirkevag, A., Seland, Ø., … Kristjánsson, J. E. (2013). The Norwegian Earth System Model, NorESM1-M—part I: Description and basic evaluation of the physical climate. *Geoscientific Model Development*, *6*(3), 687–720. https://doi.org/10.5194/gmd-6-687-2013

Bopp, L., Resplandy, L., Orr, J. C., Doney, S. C., Dunne, J. P., Gehlen, M., … Vichi, M. (2013). Multiple stressors of ocean ecosystems in the 21st century: Projections with CMIP5 models. *Biogeosciences*, *10*(10), 6225–6245. https://doi.org/10.5194/bg-10-6225-2013

Chen, S.-N. (2014). Enhancement of alongshore freshwater transport in surface-advected river plumes by tides. *Journal of Physical Oceanography*, *44*(11), 2951–2971. https://doi.org/10.1175/JPO-D-14-0008.1

Csanady, G. T. (1971). Baroclinic boundary currents and long edge-waves in basins with sloping shores. *Journal of Physical Oceanography*, *1*(2), 92–104. https://doi.org/10.1175/1520-0485(1971)001%3C0092:BBCALE%3E2.0.CO;2

Dufresne, J.-L., Foujols, M.-A., Denvil, S., Caubel, A., Marti, O., Aumont, O., … Vuichard, N. (2013). Climate change projections using the IPSL-CM5 earth system model: From CMIP3 to CMIP5. *Climate Dynamics*, *40*(9-10), 2123–2165. https://doi.org/10.1007/s00382-012-1636-1

Dunne, J. P., John, J. G., Adcroft, A. J., Griffies, S. M., Halberg, R. W., Shevliakova, E., … Zadeh, N. (2012). GFDL's ESM2 global coupled climate-carbon Earth system models. Part I: Physical formulation and baseline simulation characteristics. *Journal of Climate*, *25*, 6646–6665.

Dunne, J. P., John, J. G., Shevliakova, E., Stouffer, R. J., Krasting, J. P., Malyshev, S. L., … Zadeh, N. (2013). GFDL's ESM2 global coupled climate-carbon Earth system models. Part II: Carbon system formulation and baseline simulation characteristics. *Journal of Climate*, *26*, 2247–2267.

Fong, D. A., & Geyer, W. R. (2002). The alongshore transport of freshwater in a surface-trapped river plume. *Journal of Physical Oceanography*, *32*(3), 957–972. https://doi.org/10.1175/1520-0485(2002)032%3C0957:TATOFI%3E2.0.CO;2

Garvine, R. W. (2001). The impact of model configuration in studies of buoyant coastal discharge. *Journal of Marine Research*, *59*(2), 193–225. https://doi.org/10.1357/002224001762882637

Garvine, R. W., & Whitney, M. M. (2006). An estuarine box model of freshwater delivery to the Coastal Ocean for use in climate models. *Journal of Marine Research*, *64*(2), 173–194. https://doi.org/10.1357/002224006777606506

Gent, P. R., Danabasoglu, G., Donner, L. J., Holland, M. M., Hunke, E. C., Jayne, S. R., … Zhang, M. (2011). The Community Climate System Model version 4. *Journal of Climate*, *24*(19), 4973–4991. https://doi.org/10.1175/2011JCLI4083.1

Giorgetta, M. A., Jungclaus, J., Reick, C. H., Legutke, S., Bader, J., Böttinger, M., … Stevens, B. (2013). Climate and carbon cycle changes from 1850 to 2100 in MPI-ESM simulations for the Coupled Model Intercomparison Project Phase 5. *Journal of Advances Earth Systems*, *5*(3), 572–597. https://doi.org/10.1002/jame.20038

Haidvogel, D., Arrango, H., Budgell, W., Cornuelle, B., Curchitser, E., Lorenzo, E. D., … Wilkin, J. (2008). Ocean forecasting in terrain-following coordinates: Formulation and skill assessment of the Regional Ocean Modelling System. *Journal of Computational Physics*, *227*(7), 3595–3624. https://doi.org/10.1016/j.jcp.2007.06.016

Hetland, R. D. (2005). Relating river plume structure to vertical mixing. *Journal of Physical Oceanography*, *35*(9), 1667–1688. https://doi.org/10.1175/JPO2774.1

Hill, A. E. (1998). Buoyancy effects in coastal and shelf seas. In K. H. Brink & A. R. Robinson (Eds.), *The sea* (Vol. 10, pp. 21–26). Hoboken, NJ: John Wiley.

Horner-Devine, A., Hetland, R. D., & MacDonald, D. G. (2015). Mixing and transport in coastal river plumes. *Annual Review of Fluid Mechanics*, *47*(1), 569–594. https://doi.org/10.1146/annurev-fluid-010313-141408

Horner-Devine, A. R., Fong, D. A., Monismith, S. G., & Maxworthy, T. (2006). Laboratory experiments simulating a coastal river inflow. *Journal of Fluid Mechanics*, *555*, 203–232. https://doi.org/10.1017/S0022112006008937

Ilyina, T., Six, K. D., Segschneider, J., Maier-Reimer, E., Li, H., & Núñez-Riboni, A. I. (2013). Global ocean biogeochemistry model HAMOCC: Model architecture and performance as a component of the MPI-Earth system model in different CMIP5 experimental realizations. *Journal of Advances in Modeling Earth Systems*, *5*, 2870315.

Isobe, A. (2005). Ballooning of river-plume bulge and its stabilization by tidal currents. *Journal of Physical Oceanography*, *35*(12), 2337–2351. https://doi.org/10.1175/JPO2837.1

Izett, J., & Fennel, K. (2018). Estimating the cross-shelf export of riverine materials: Part 2. Estimates of global freshwater and nutrient export. *Global Biogeochemical Cycles*, *32*. https://doi.org/10.1002/2017GB005667

Jurisa, J. T., & Chant, R. J. (2013). Impact of offshore winds on a buoyant river plume system. *Journal of Physical Oceanography*, *43*(12), 2571–2587. https://doi.org/10.1175/JPO-D-12-0118.1

Kara, A. B., Wallcraft, A. J., Metzger, E. J., Hurlburt, H. E., & Fairall, C. W. (2007). Wind stress drag coefficient over the Global Ocean. *Journal of Climate*, *20*(23), 5856–5864. https://doi.org/10.1175/2007JCLI1825.1

Kourafalou, V. H., Oey, L.-Y., Wang, J. D., & Lee, T. N. (1996). The fate of river discharge on the continental shelf. 1. Modelling the river plume and the inner shelf coastal current. *Journal of Geophysical Research*, *101*, 3415–3434.

Laruelle, G. G., Robeix, V., Sferratore, A., Brodherr, B., Ciuffa, D., Conley, D. J., … Van Cappellen, P. (2009). Antrhopogenic perturbations of the silicon cycle at the global scale: Key role of the land-ocean transition. *Global Biogeochemical Cycles*, *23*, GB4031. https://doi.org/10.1029/2008GB003267

Lehrter, J. C., Ko, D. S., Murrell, M. C., Hagy, J. D., Schaeffer, B. A., Greene, R. M., … Penta, B. (2013). Nutrient distributions, transports, and budgets on the inner margin of a river-dominated continental shelf. *Journal of Geophysical Research: Oceans*, *118*, 1–17. https://doi.org/10.1002/jgrc.20362

Ludwig, W., Probst, J.-L., & Kempe, S. (1996). Predicting the oceanic input of organic carbon by continental erosion. *Global Biogeochemical Cycles*, *10*, 23–41. https://doi.org/10.1029/95GB02925

McCreary, J. P., Zhang, S., & Shetye, S. R. (1997). Coastal circulations driven by river outflow in a variable-density 1 1/2-layer model. *Journal of Geophysical Research*, *102*, 15,535–15,554. https://doi.org/10.1029/97JC00985

Moore, J. K., Lindsay, K., Doney, S. C., Long, M. C., & Misumi, K. (2013). Marine ecosystem dynamics and biogeochemical cycling in the Community Earth System Model [CESM1(BGC)]: Comparison of the 1990s with the 2090s under the RCP4.5 and RCP8.5 scenarios. *Journal of Climate*, *26*(23), 9291–9312. https://doi.org/10.1175/JCLI-D-12-00566.1

Oey, L.-Y., & Mellor, G. L. (1992). Subtidal variability of estuarine outflow, plume, and coastal current: A model study. *Journal of Physical Oceanography*, *23*, 164–171.

Palmer, J. R., & Totterdell, I. J. (2001). Production and export in a global ocean ecosystem model. *Deep Sea Research*, *48*(5), 1169–1198. https://doi.org/10.1016/S0967-0637(00)00080-7

Rabouille, C. F., Mackenzie, T., & Ver, L. M. (2001). Influence of the human perturbation on carbon, nitrogen, and oxygen on biogeochemical cycles in the global coastal ocean. *Geochimica et Cosmochimica Acta*, *65*(21), 3615–3641. https://doi.org/10.1016/S0016-7037(01)00760-8

Seitzinger, S. P., Harrison, A., Dumont, E., Beusen, A. H., & Bouwman, A. F. (2005). Sources and delivery of carbon, nitrogen, and phosphorus to the coastal zone: An overview of Global Nutrient Export from Watersheds (NEWS) models and their application. *Global Biogeochemical Cycles*, *19*, GB4S01. https://doi.org/10.1029/2005GB002606

Sharples, J., Middelburg, J. J., Fennel, K., & Jickells, T. D. (2017). What proportion of riverine nutrients reaches the open ocean? *Global Biogeochemical Cycles*, *31*, 39–58. https://doi.org/10.1002/2016GB005483

Tjiputra, J. F., Roeland, C., Bentsen, M., Lawrence, D. M., Lorentzen, T., Schwinger, J., … Heinze, C. (2013). Evaluation of the carbon cycle components in the Norwegian Earth System Model (NorESM). *Geoscientific Model Development*, *6*(2), 301–325. https://doi.org/10.5194/gmd-6-301-2013

Vichi, M., Manzini, E., Fogli, P. G., Alessandri, A., Pantara, L., Scoccimarro, E., … Navarra, A. (2011). Global and regional ocean carbon uptake and climate change: Sensitivity to a substantial mitigation scenario. *Climate Dynamics*, *37*(9-10), 1929–1947. https://doi.org/10.1007/s00382-011-1079-0

Vichi, M. S., Masina, S., & Navarra, A. (2006). A generalized model of pelagic biogeochemistry for the global ocean ecosystem. Part II: Numerical simulations. *Journal of Marine Systems*, *64*, 110–134.

Volodin, E. M., Dianskii, N. A., & Gusev, A. V. (2010). Simulating present-day climate with the INMCM4.0 coupled model of the atmospheric and oceanic general circulations. *Izvestiya Atmospheric and Oceanic Physics*, *46*, 448–466.

Watanabe, S., Hajima, T., Sudo, K., Nagashima, T., Takemura, T., Okajima, H., … Kawamiya, M. (2011). MIROC-ESM 2010: Model description and basic results of CMIP5-20c3m experiments. *Geoscientific Model Development*, *4*(4), 845–872. https://doi.org/10.5194/gmd-4-845-2011

Yankovsky, A. E., & Chapman, D. C. (1997). A simple theory for the fate of buoyant coastal discharges. *Journal of Physical Oceanography*, *27*(7), 1386–1401. https://doi.org/10.1175/1520-0485(1997)027%3C1386:ASTFTF%3E2.0.CO;2